Modeling and Optimization of Phenolic Compound Adsorption from Olive Wastewater Using XAD-4 Resin, Activated Carbon, and Chitosan Biosorbent

Chaimaa Hakim, Hélène Carrère, Abdessadek Essadek, Soukaina Terroufi, Audrey Battimelli, Renaud Escudie, Jérôme Harmand, Mounsef Neffa

applied sciences

MDPI

Article

Modeling and Optimization of Phenolic Compound Adsorption from Olive Wastewater Using XAD-4 Resin, Activated Carbon, and Chitosan Biosorbent

Chaimaa Hakim [1,2,3], Hélène Carrère [2,*], Abdessadek Essadek [1,3], Soukaina Terroufi [1], Audrey Battimelli [2], Renaud Escudie [2], Jérôme Harmand [2] and Mounsef Neffa [1,3,*]

[1] Laboratory of Bioresources, Biotechnology, Ethnopharmacology and Health, University Mohammed Premier, Oujda 60000, Morocco; chaimaa.hakim@inrae.fr (C.H.)
[2] Laboratory of Environmental Biotechnology, French National Research Institute for Agriculture, Food & Environment, Montpellier University, 11100 Narbonne, France
[3] Center for Biomass Valorization and Environmental Protection, Technopole of Mohammed First University, Oujda 60000, Morocco
* Correspondence: helene.carrere@inrae.fr (H.C.); m.neffa@ump.ac.ma (M.N.)

Featured Application

This research applies a "double-green" circular economy strategy by valorizing shrimp shell waste to treat olive mill wastewater. The developed chitosan biosorbent efficiently recovers bioactive phenolic compounds, offering a sustainable industrial solution for the detoxification of effluents and the production of high-value extracts for pharmaceutical, cosmetic, and food applications.

Abstract

This study proposes a circular economy strategy to recover phenolic compounds by valorizing shrimp shell waste into a chitosan biosorbent (CH-B). Its adsorption efficiency was evaluated compared to commercial activated carbon (AC) and synthetic XAD-4 resin. Kinetic analysis revealed that while both pseudo-first-order (PFO) and pseudo-second-order (PSO) models exhibited high correlations ($R^2 \geq 0.96$), both CH-B and XAD-4 resin were best described by the PFO model. This aligns with diffusion-controlled processes consistent with the porous and physical nature of these adsorbents. In contrast, AC followed the PSO model. Isotherm modeling indicated that CH-B and AC fit the Temkin model, reflecting heterogeneous surfaces, whereas XAD-4 followed the Langmuir model (monolayer adsorption). Notably, CH-B exhibited a maximum adsorption capacity (q_m) of 229.2 mg/g, significantly outperforming XAD-4 (104.8 mg/g) and AC (90.2 mg/g). Thermodynamic and kinetic modeling confirmed that the adsorption mechanism was governed by a combination of electrostatic interactions, π–π stacking, and hydrogen bonding between the hydroxyl/amine groups of chitosan and phenolic compounds. Optimization using Box–Behnken design for CH-B showed optimal acidic pH and moderate temperature but non-significant effect of CH-B dose in the experimental domain. Optimisation results showed unexpected high removal efficiency at low CH-B dosages. A tentative explanation may be adsorbent aggre-gation, which needs to be confirmed by further experimental evidence.

Keywords: olive mill wastewater; phenolic compounds; adsorption; Box–Behnken design; chitosan biosorbent; kinetic and isotherm modeling

Academic Editor: Heonseop Eom

Received: 18 December 2025
Revised: 19 January 2026
Accepted: 21 January 2026
Published: 25 January 2026

1. Introduction

Olive oil production for the 2024–2025 season is expected to exceed 3.5 million tons, reflecting an increase of nearly 37% compared with the previous year's low harvest and around 17% above the past five years' average [1]. This growing production is accompanied by substantial quantities of olive mill wastewater (OMWW), generated at 3–3.5 m^3 per ton of olive oil, which corresponds to an estimated 10–12 million m^3 of effluents annually. OMWW is characterized by a very high organic load, significant chemical oxygen demand (COD), acidic pH, and limited biodegradability. These features make its disposal a persistent environmental challenge [2]. Among its constituents, phenolic compounds are of particular concern due to their toxicity, resistance to microbial degradation, and inhibitory effects on biological treatment processes. However, these bioactive molecules possess a high antioxidant value, offering possibilities for their extraction and potential use in the pharmaceutical, cosmetic, and food industries [3]. This dual nature as both a pollutant and a resource has stimulated interest in treatment strategies capable of reducing environmental risk while enabling the recovery of valuable compounds [4].

Among the various approaches explored, adsorption has gained a growing role as an efficient and relatively simple process for treating OMWW, particularly because of its adaptability and cost-effectiveness when dealing with complex effluents [5,6]. A wide range of adsorbent materials has been investigated, ranging from synthetic polymeric materials to bio-based sorbents. In particular, XAD-4 resin, activated carbon (AC), and chitosan biosorbents have attracted particular attention owing to their contrasting surface chemistries and their proven ability to retain phenolic compounds. XAD-4 resin is a hydrophobic polystyrene–divinylbenzene polymer distinguished by its strong mechanical and chemical stability across a wide range of operating conditions, which supports its use in intensive treatment processes [7]. Activated carbon (AC) remains widely applied due to its developed porosity and high surface area, enabling the retention of a broad spectrum of organic pollutants [8]. Recently, biopolymer-based sorbents have attracted growing attention as environmentally friendly alternatives in recent years [9]. Among these, chitosan, obtained by N-deacetylation of chitin from crustacean shells, is particularly promising because it is biodegradable, easily modified, and relatively inexpensive [10]. Utilizing chitosan derived from shrimp shell waste to treat agro-industrial waste (OMWW) represents a double-green circular economy strategy, as it simultaneously valorizes two distinct waste streams. Furthermore, the amino and hydroxyl functional groups of chitosan offer numerous reactive sites, and several studies have demonstrated its effectiveness in capturing polyphenols from OMWW [11].

A detailed analysis of adsorption performance requires an understanding of both equilibrium and rate processes. Adsorption isotherms provide insight into the interactions between solutes and sorbent surfaces [12], while kinetic models help identify the steps governing mass transfer and adsorption rates [13]. Since system performance is highly dependent on pH, temperature, and adsorbent dosage that often interact non-linearly, statistical optimization tools are essential. In particular, the Box–Behnken design (BBD) has proven valuable for investigating combined parameter effects while minimizing the number of experiments required. Several recent studies illustrate this potential [14]: Fseha et al. [15] reported up to 94% phenol removal using date-palm-derived biochar, while Elayadi et al. [16] achieved more than 90% polyphenol removal using sugarcane bagasse. These works underscore the capacity of BBD to enhance adsorption efficiency while revealing significant interactions among operating variables.

While recent studies have explored chitin, insect-based chitosan [17], and chitosan derivatives [18], or chemically modified nanocomposites [19] for the recovery of phenolic compounds from olive mill waste waters, these approaches are often limited by matrix com-

plexity or the use of toxic cross-linkers. In contrast, this study validates a "double-green" circular economy approach using pure, unmodified crustacean chitosan. Furthermore, our integrated approach represents a significant practical advancement by directly comparing and optimizing the performance of this sustainable biosorbent against established industrial benchmarks (XAD-4, AC) for the treatment of real OMWW.

In this context, the present study examines the adsorption of total phenolic compounds (TPhCs) from OMWW using three adsorbent materials: XAD-4 resin, activated carbon (AC), and a chitosan biosorbent (CH-B). Adsorption kinetics and equilibrium behavior were examined to better understand the mechanisms governing TPhC uptake and to support the development of sustainable treatment and resource recovery strategies. The Box–Behnken design was further employed to evaluate the individual and combined effects of key operational variables, enabling the identification of optimal conditions for maximizing the adsorption efficiency.

2. Materials and Methods

2.1. Sample Collection and Materials

OMWW was collected during the olive oil production season of 2024 from a traditional extraction unit located in Oujda, Morocco. Upon collection, the effluent was transferred into sealed high-density polyethylene containers and stored at 4 °C to preserve its physicochemical characteristics prior to experimental use. Before use, the raw OMWW was filtered through standard filter paper and diluted to 50% (v/v) with distilled water. Three adsorbents were selected for the removal of total phenolic compounds (TPhCs): Amberlite XAD-4 resin, activated carbon (AC), and chitosan biosorbent (CH-B). Both commercial adsorbents (Amberlite™ XAD-4 resin and AC) were purchased from Sigma-Aldrich (St. Louis, MI, USA). Commercial powdered activated carbon, particle size 100 mesh, BET surface area (~600 m^2/g) was used as a reference material, while the macroreticular polymeric resin (Amberlite™ XAD-4) exhibited a surface area of 750 m^2/g.

Prior to use, the XAD-4 resin was soaked in acetone for 8 h under rotary agitation at room temperature to remove impurities and activate the sorption sites. The chitosan biosorbent (CH-B) was synthesized from brown shrimp shell waste collected from a local seafood processing plant in Morocco. The shells were first washed, dried, and milled to achieve a particle size of 0.45 mm. Chitosan was subsequently extracted through successive demineralization, deproteinization, and deacetylation steps, as described in the following section. All the reagents used were of analytical grade and employed without further purification.

2.2. Extraction and Preparation of Chitosan Biosorbent

Chitosan was extracted from brown shrimp shells following three successive steps: demineralization, deproteinization, and deacetylation, adapted from the procedure described by Dahmane et al. [20], with minor methodological adjustments. In the demineralization step, the ground shrimp shell powder was treated with 0.25 M hydrochloric acid (HCl) at a solid-to-liquid ratio of 1:40 (w/v) for 2 h at room temperature. The solid fraction was subsequently recovered by filtration, thoroughly rinsed with distilled water until neutral pH, and then dried at 60 °C. Deproteinization was carried out by treating the demineralized shells with 1 M sodium hydroxide (NaOH) solution at a solid-to-liquid ratio of 1:20 (w/v) under continuous agitation at 250 rpm for 24 h. The resulting chitin was separated, rinsed repeatedly with distilled water, and dried. The final step, deacetylation, was performed to convert chitin into chitosan. The dried chitin samples were treated with 50% (w/v) NaOH solution at a solid-to-liquid ratio of 1:20 (w/v) and heated at 70 °C for 3 h. After deacetylation, the chitosan was filtered and thoroughly washed with distilled

water until the pH reached neutrality. The purified chitosan was then dried at 60 °C for 20 h, ground to a particle size of 0.45 mm, and stored at room temperature for subsequent characterization and adsorption experiments.

2.3. Characterization of OMWW and Adsorbents

The physicochemical characterization of the raw and filtered OMWW was performed following the standard methods outlined by the American Public Health Association (APHA). The analysis included the determination of total solids (TS), volatile solids (VS), and pH. Total chemical oxygen demand (TCOD) was measured using Aqualitic COD tubes (0–1500 mg O_2/L). For each analysis, 0.5 g of the sample was hydrolyzed with 20 mL of concentrated sulfuric acid (H_2SO_4) and digested overnight to ensure the complete oxidation of organic matter. A 2 mL aliquot of the diluted hydrolyzed sample was then transferred to spectroquant test kits, with Milli-Q water used as a blank. The final digestion was carried out in a HACH COD reactor at 150 °C for 2 h with potassium dichromate under acidic conditions. After cooling to room temperature, absorbance was read at 620 nm using a HACH DR/2000 spectrophotometer (Hach Company, Loveland, CO, USA) [21]. The concentration of total polyphenolic compounds (TPhCs), expressed as mg/L of gallic acid equivalent (GAE), was analyzed according to the Folin–Ciocalteu method [22]. For this assay, 20 µL of each diluted sample was mixed with 500 µL of diluted Folin–Ciocalteu reagent and 400 µL of 20% (*w*/*w*) sodium carbonate (Na_2CO_3) solution. The mixtures were incubated at 35 °C for 20 min, after which absorbance was measured at 760 nm by a multifunctional microplate reader. All the basic analytical measurements, including TPhC and physicochemical parameters, were performed in triplicate (n = 3), with the results expressed as mean ± standard deviation. The adsorbents XAD-4 resin, AC, and CH-B were characterized before and after adsorption by elemental analysis (PerkinElmer 2400 Series II CHNS analyzer, PerkinElmer, Waltham, MA, USA), FT-IR spectroscopy (Thermo Scientific Nicolet iS10, 4000–400 cm^{-1}, 4 cm^{-1} resolution, Waltham, MA, USA), and Scanning Electron Microscopy (SH-5500P Tabletop SEM, Hirox, Tokyo, Japan, 10 kV, high vacuum, SED mode).

2.4. Adsorption Kinetics and Isotherms

2.4.1. Kinetics of Adsorption

Kinetic studies were conducted to understand the adsorption rate and mechanism of TPhC from OMWW onto the selected adsorbents. In each experiment, a defined mass of dried adsorbent was added to 50 mL of diluted OMWW (prepared by mixing equal volumes of OMWW and distilled water, i.e., 50% (*v*/*v*)). The flasks were then agitated in a horizontal shaker operating at 200 rpm, and samples were withdrawn at predetermined time intervals to determine the residual TPhC concentration.

The pseudo-first-order (1), pseudo-second-order (2), and Elovich's kinetic models (3) were used to describe the best fit of the experimental data obtained from TPhC adsorption. The experimental sorption data were fitted to the non-linear form of the models.

The pseudo-first-order kinetic model (Lagergren's equation) assumes that the rate of adsorption is proportional to the number of unoccupied sites on the adsorbent surface. This model is often associated with physisorption processes, where adsorption is primarily governed by weak interactions such as van der Waals forces or hydrogen bonding [23], and is expressed in Equation (1):

$$q_t = q_e\left(1 - e^{-k_1 t}\right) \quad (1)$$

where q_e and q_t (mg/g) represent the adsorption capacities at equilibrium and at time t (min), respectively. k_1 (1/min) is the pseudo-first-order rate constant.

The pseudo-second-order kinetic model is based on the assumption that chemisorption is the rate-limiting step involving valence forces [24]. It is expressed as follows (Equation (2)):

$$q_t = \frac{K_2 q_e^2 t}{1 + K_2 q_e t} \quad (2)$$

where K_2 g/(mg.min) is the pseudo-second-order rate constant,.

The Elovich kinetic model, often applied to chemisorption processes on heterogeneous surfaces [25], is expressed as

$$q_t = \frac{1}{b} \ln(1 + abt) \quad (3)$$

where a is the initial adsorption rate constant mg/(g.min), and b is the desorption or surface coverage constant of the Elovich model (g/mg).

2.4.2. Adsorption Isotherms

In each experiment, 1 g of XAD-4 resin or AC and 100 mg of CH-B were separately added to 50 mL of diluted OMWW solution (prepared as a 1:1 v/v mixture of OMWW and distilled water) in 100 mL flasks. A lower mass of CH-B (100 mg) was employed compared to the commercial adsorbents (1 g) based on preliminary trials. This adjustment was necessitated by the biosorbent's significantly lower bulk density and higher specific adsorption capacity, ensuring both effective hydrodynamic mixing and accurate equilibrium data collection. The mixtures were agitated on an orbital shaker at 200 rpm and room temperature for 1 h to ensure equilibrium was reached. After adsorption, the adsorbents were removed by filtration, and the supernatants were analyzed for residual TPhC content using the Folin–Ciocalteu method.

The equilibrium adsorption capacity (q_e, mg/g) was calculated according to the following equation (Equation (4)):

$$q_e = \frac{(C_e - C_0)\, V}{m} \quad (4)$$

where C_e and C_0 represent the equilibrium and initial TPhC concentrations in solutions (mg/L), m is the mass of adsorbent (g), and V denotes the volume of the solution (L). To describe and compare the adsorption behavior of the three adsorbents. Three equilibrium isotherm models were applied to the experimental data: Langmuir (5), Freundlich (7), and Temkin (8).

The Langmuir model assumes monolayer adsorption on a uniform surface with a finite number of adsorption sites, and that all the adsorption sites have the same sorption activation energy (Equation (5)).

$$q_e = \frac{q_m K_L C_e}{1 + K_L C_e} \quad (5)$$

where q_m (mg/g) indicates the maximum adsorption capacity and K_L (L/mg) represents the Langmuir constant related to the affinity of the binding sites [26]. Moreover, the dimensionless separation factor RL (Equation (6)) indicates whether the adsorption process is favorable ($0 < R_L < 1$), unfavorable ($R_L > 1$), linear ($R_L = 1$), or irreversible ($R_L = 0$):

$$R_L = \frac{1}{1 + K_L C_0} \quad (6)$$

The Freundlich isotherm was derived from the assumption that adsorption occurs on a heterogeneous surface through a multilayer adsorption mechanism (Equation (7)):

$$q_e = K_F C_e^{\frac{1}{n}} \quad (7)$$

where K_F is the constant of the Freundlich model with a unit of $(mg/g)(L/mg)^{1/n}$. The value of $1/n$ represents the intensity of adsorption or surface heterogeneity, indicating the energy distribution relative to the adsorbate sites and heterogeneity. When $0 < 1/n < 1$, the adsorption is favorable. When $1/n > 1$, it suggests unfavorable adsorption, while $1/n = 1$ indicates a linear adsorption isotherm. As $1/n$ approaches 0, the isotherm becomes increasingly irreversible. The irreversibility of the isotherm can be attributed to the fact that pressure or concentration must decrease to a very low value prior to the desorption of adsorbate molecules from the surface [27].

The Temkin isotherm considers the adsorbate–adsorbent interactions, assuming that the heat of adsorption decreases linearly with increasing surface coverage [28]. It is expressed as Equation (8):

$$q_e = \frac{q_m RT}{b_T} \ln K_T C_e = q_T \ln K_T C_e \quad (8)$$

where q_e (mg/g) is the equilibrium adsorption capacity, C_e (mg/L) is the equilibrium solute concentration, q_m (mg/g) is the maximum adsorption capacity, R is the universal gas constant (8.314 J/mol/K), T is the absolute temperature (K), b_T (J/mol) is the Temkin constant related to adsorption heat, and K_T (L/mg) is the equilibrium binding constant. The parameter q_T (mg/g) is a lumped parameter characterizing the adsorption capacity normalized by the binding energy.

All the model parameters were calculated using non-linear regression analysis with Origin 8.0 software (OriginLab, Northampton, MA, USA). While the coefficient of determination (R^2) was computed to assess the overall correlation, relying solely on this metric is often insufficient for discriminating between non-linear models, particularly when multiple equations lead to similar high correlations [29]. Therefore, to rigorously identify the most suitable model and avoid statistical bias, the Akaike Information Criterion (AIC, Equation (9)) and Bayesian Information Criterion (BIC, Equation (10)) were employed as the decisive selection criteria. As highlighted by Vareda et al. [30], these criteria provide a more robust assessment by weighing the goodness of fit against the complexity of the model (number of parameters), thus minimizing information loss and preventing overfitting. The AIC and BIC values were calculated using the following equations:

$$AIC = N \times \ln\left(\frac{RSS}{N}\right) + 2p \quad (9)$$

$$BIC = N \times \ln\left(\frac{RSS}{N}\right) + p\ln(N) \quad (10)$$

where N represents the number of experimental data points, RSS is the residual sum of squares, and p is the number of adjustable model parameters. The model exhibiting the lowest AIC and BIC values was selected as the best descriptor for the adsorption process.

2.4.3. Experimental Design and Optimization of Adsorption Experiments by RSM

Response Surface Methodology (RSM) was applied to investigate the influence of key operational parameters on the adsorption of TPhC from OMWW. Among the different RSM approaches, the Box–Behnken design (BBD) was selected for its efficiency for modeling non-linear responses with a limited number of experiments [31]. Three independent variables were considered: adsorbent dosage (X_1), effluent pH (X_2), and temperature (X_3). The

experimental matrix consisted of 15 runs, including three replicates at the central point to estimate pure error and ensure reproducibility, and statistical significance was assessed via ANOVA. Each factor was tested at three coded levels (−1, 0, +1), as summarized in Table 1. The pH of the OMWW solutions was adjusted to the target levels using negligible volumes of 1 M HCl or 1 M NaOH to prevent significant dilution. Temperature control was achieved using a temperature-controlled orbital shaker. To ensure thermal equilibrium, the samples were incubated at the specified temperature for 20 min prior to the addition of the adsorbent.

Table 1. Actual and coded levels of factors for Box–Behnken design (BBD).

Experimental Variable		Coded Levels and Values		
		−1	**0**	**1**
A: Temperature (°C)		25	37.5	50
B: pH		2	5	8
C: Adsorbent dosage (g/L)	XAD-4 resin, AC	20	60	100
	CH-B	2	5	8

Given the differences in effective dosage ranges across adsorbents, XAD-4 resin and AC were tested at concentrations of 20, 60, and 100 g/L, whereas the CH-B was evaluated at 2, 5, and 8 g/L. The experimental design, regression analysis, and analysis of variance (ANOVA) were performed using Design-Expert software (version 13, Stat-Ease Inc., Minneapolis, MN, USA).

The experimental data were analyzed using Response Surface Methodology (RSM). While the data were initially fitted to a second-order polynomial equation, the analysis indicated the significance of higher-order interactions. Consequently, a reduced cubic model was applied to optimize the model's predictive capability [32]. This model includes linear, quadratic, and specific cubic interaction terms and is expressed by the following general equation (Equation (11)):

$$Y = x_0 + \sum_{i=1}^{3} \beta_i X_i + \sum_{i=1}^{3} \beta_{ii} {X_i}^2 + \sum_{i=1}^{2} \sum_{j=i+1}^{3} \beta_{ij} X_i X_j + \sum_{i=1}^{3} \sum_{j \neq i}^{3} \beta_{iij} {X_i}^2 X_j + \varepsilon \quad (11)$$

Y represents the predicted TPhC adsorption yield (%); x_0 is the intercept; X_i, X_j, and X_k represent the coded input factors (A, B, and C); β_i, β_{ii}, β_{ij}, and β_{iij} are the linear, quadratic, interaction, and cubic interaction coefficients, respectively; and ε is the random error term. [33].

The TPhC adsorption yield (%) was calculated using the following formula (Equation (12)):

$$\text{TPhC adsorption yield}(\%) = \frac{(C_0 - C_e)}{C_0} \times 100 \quad (12)$$

where C_0 and C_e are the initial and equilibrium concentrations of phenolic compounds, respectively.

The experimental and predicted adsorption yields for XAD-4 resin and activated carbon are presented in Table S1, while the results for CH-B are shown in Table S2.

3. Results and Discussion

3.1. Characterization of OMWW

The physicochemical characterization of raw OMWW and the filtered effluent is reported in Table 2. The pH remained stable at 5 after filtration, indicating no significant

change in acidity. The TCOD declined from 260 ± 6 g O_2/L to 243 ± 2 g O_2/L, representing a decrease of 6.54%. Total solids reduced from 145 ± 4 g/L to 138 ± 2 g/L (4.83% reduction), while total volatile solids decreased from 111 ± 3 g/L to 104 ± 4 g/L, corresponding to a 6.31% loss. The total phenolic content decreased from 8 ± 1 g/L to 7 ± 2 g/L, corresponding to an approximate 12.5% reduction, which was slightly higher than the variations observed for the other parameters. These findings align with other studies revealing that olive mill effluents tend to be acidic, with a high load of organic matter, and rich in phenolic compounds [34]. Such characteristics highlight the need for integrated treatment strategies, such as adsorption, that can handle acidic pH and high organic loads while enabling phenolic recovery for valorization purposes [35]. Consequently, selecting a suitable adsorbent tailored to the specific physicochemical properties of OMWW is essential for achieving efficient and sustainable treatment performance.

Table 2. Physicochemical characterization of raw and filtered OMWW (mean (3) ± standard deviation).

Parameters	Raw OMWW	Filtered OMWW
pH (25 °C)	5.1	5.03
TCOD (gO_2/L)	260 ± 6	243 ± 2
Total solids(g/L)	145 ± 4	138 ± 2
Total volatile solids (g/L)	111 ± 3	104 ± 4
Total phenolic compounds (g/L)	8 ± 1	7 ± 2

3.2. Characterization of the Adsorbents Before and After TPhC Adsorption from OMWW

3.2.1. Elemental Analysis

The elemental composition of the adsorbents XAD-4 resin, activated carbon (AC), and CH-B was determined before and after adsorption of TPhC (Table 3). AC exhibited a moderate carbon content (68%) and a substantially higher oxygen content (31%), indicating the presence of surface oxygenated functionalities resulting from the activation process. These oxygenated groups enhance surface polarity and potential hydrogen bonding, thereby contributing to the affinity of phenolic compounds [36]. Prior to adsorption, XAD-4 resin exhibited a high carbon content (90%), with negligible nitrogen and minor oxygen (1%), consistent with its hydrophobic polystyrene–divinylbenzene structure. This elemental profile confirms the absence of polar functional groups, suggesting that adsorption on XAD-4 occurs predominantly through non-specific interactions, including π–π stacking or hydrophobic forces [37]. In comparison, the CH-B displayed a distinct elemental profile, with a lower carbon content (42%) but significantly higher oxygen (46%) and nitrogen (6%) contents. These values are consistent with the presence of hydroxyl (–OH) and amine (–NH_2) groups, which are known to facilitate strong hydrogen bonding and electrostatic interactions with phenolic molecules [38].

Table 3. Elemental composition (%) of AC, XAD-4 resin, and CH-B before and after adsorption (*w*/*w* %, dry basis).

Element	AC	XAD-4 Resin	CH-B	AC	XAD-4 Resin	CH-B
	Before Adsorption			After Adsorption		
	Weight Percent (*w*/*w* %)					
C	68.0	90.0	41.8	73.8	70.7	73.8
N	0.5	-	6.0	1.1	1.1	1.5
O	30.6	1.0	46.5	22.7	26.4	22.7
H	0.9	9.0	5.7	2.0	1.8	2.0

Following TPhC adsorption, the elemental composition of all the adsorbents changed, particularly for AC and CH-B. Specifically for AC, the carbon content increased to 71%, while the oxygen content decreased to 26%. Similarly, for CH-B, the carbon content rose to 74% and oxygen dropped to 23%, indicating surface modification driven by the adsorption of organic compounds from OMWW.

3.2.2. FTIR Analysis

The FTIR analysis revealed distinct adsorption mechanisms for AC, XAD-4 resin, and CH-B in the removal of TPhC from OMWW (Figure 1). Based on the specific spectral bands observed, the proposed binding interactions are schematically illustrated in Figure 2. For AC, spectral changes were detected in the bands corresponding to C–H, C=O, and C–O stretching variations (~1000–1200 cm^{-1}), indicating the involvement of oxygen-containing surface functional groups in the adsorption process. These spectral variations suggest that adsorption proceeds primarily through π–π interactions and hydrogen bonding with oxygenated surface groups of AC. These findings are consistent with prior studies that highlight AC's effectiveness in adsorbing phenolics through its aromatic and porous structure [39].

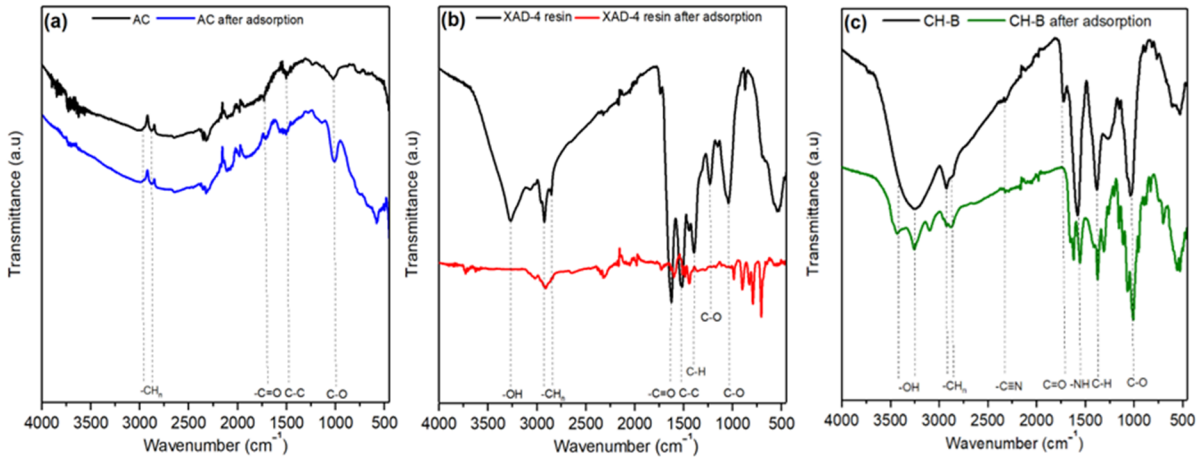

Figure 1. FTIR spectrum of (**a**) AC, (**b**) XAD-4 resin, and (**c**) CH-B before and after adsorption of TPhC from OMWW.

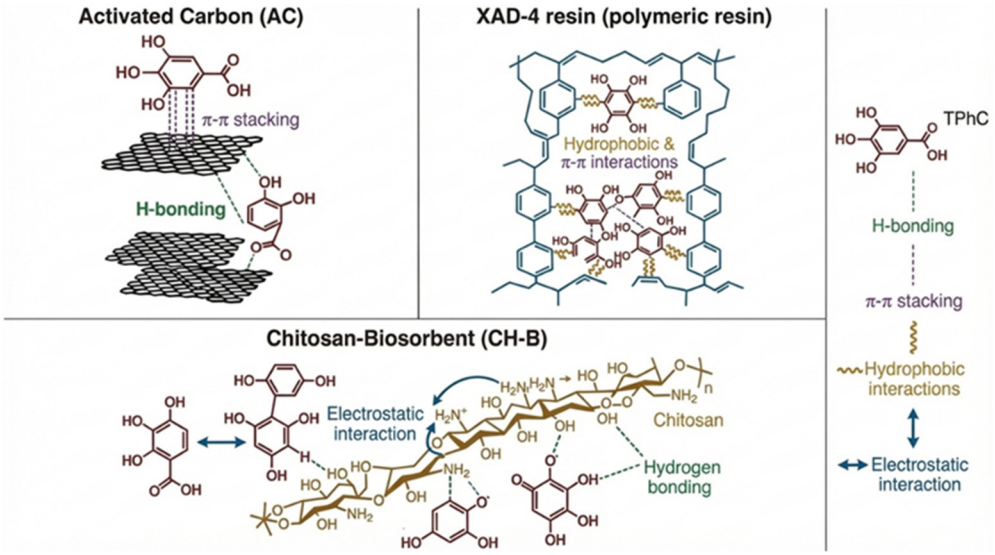

Figure 2. Molecular interaction mechanisms between phenolic compounds and three different adsorbents (AC, XAD-4, and CH-B).

For XAD-4 resin, more pronounced absorption bands were observed among the three materials. Substantial reductions in the aromatic C=C (~1600 cm^{-1}), C–H (~2920 cm^{-1}), and C=O (~1700 cm^{-1}) stretching regions, along with a broad decrease in the O-H stretching vibration (~3400 cm^{-1}) was observed after adsorption. Moreover, the decrease in the –OH band intensity suggests the displacement of physically adsorbed water molecules from the porous matrix by the phenolic compounds. The weak peaks observed in the 1000–1300 cm^{-1} region of the raw resin are attributed to C–O stretching vibrations, likely arising from minor surface oxidation or residual impurities from the synthesis process.

These spectral changes indicate that the uptake of phenolic compounds occurs primarily through π–π stacking and hydrophobic interactions with the styrene–divinylbenzene matrix, complemented by hydrogen bonding involving surface hydroxyl groups. For CH-B, distinct spectral changes were observed after adsorption. The broad O–H stretching band (~3400 cm^{-1}) significantly decreased in intensity, indicating hydrogen bonding with phenolic hydroxyl groups. The amide band C=O (~1650 cm^{-1}) became more pronounced, while the N–H bending and C–N stretching (~1550–1400 cm^{-1}) exhibited distinct shifts. Additionally, modifications in the C–O stretching region (1000–1200 cm^{-1}) confirmed the involvement of hydroxyl and amine functionalities in adsorption. These spectral variations suggest that phenolic uptake by CH-B occurs mainly through hydrogen bonding and electrostatic interactions involving the –OH and $–NH_2$ groups of chitosan, consistent with previously reported mechanisms for chitosan-based biosorbents [40].

3.2.3. Morphological Characteristics of the Used Adsorbents During Polyphenol Adsorption from OMWW

The morphological characteristics of the AC surface before and after TPhC adsorption were examined by SEM micrographs, and the results are shown in Figure 3. The raw AC surface (Figure 3a) exhibited a highly porous, fractured, and irregular structure, characterized by abundant macro- and mesopores. These textural features reflect the material's high specific surface area and accessibility of internal pore networks, which are critical for efficient adsorption. After adsorption (Figure 3b), the surface appeared smoother, with partial pore filling and the presence of adsorbed material, suggesting that phenolic molecules became deposited within the pore network and across the surface. Distinct surface changes were also observed for the XAD-4 resin before and after TPhC adsorption in the SEM images (Figure 3c,d). Initially, the resin exhibits smooth, spherical beads with a homogeneous surface, characteristic of its cross-linked polystyrene–divinylbenzene structure. After adsorption (Figure 3d), subtle surface irregularities and localized deposits appear, indicating the formation of adsorbate layers without significant structural deformation.

The morphological evolution of the biosorbent was examined via SEM (Figure 4). Raw shrimp waste (Figure 4a) exhibited a compact, layered structure with low porosity, likely due to the presence of residual proteins and minerals that restrict active site accessibility. After deacetylation, the CH-B (Figure 4b) exhibited a porous surface with ridges and fissures, thereby enhancing surface area and increasing the availability of binding sites. Following TPhC adsorption (Figure 4c), the CH-B surface appeared smoother with embedded aggregates, indicating active site occupation and surface complex formation.

3.3. Batch Adsorption Kinetics

The adsorption kinetics of TPhC onto AC, XAD-4 resin, and CH-B were analyzed using the pseudo-first-order (PFO), pseudo-second-order (PSO), and Elovich models. The kinetic parameters, along with the coefficient of determination (R^2), Akaike Information Criterion (AIC), and Bayesian Information Criterion (BIC), are summarized in Table 4. As illustrated in Figure 5, the experimental data for all the adsorbents were satisfactorily described by both the PFO and PSO models, with high coefficients of determination ($R^2 \geq 0.96$)

observed across all the systems. However, the high similarity in R^2 values precluded definitive discrimination between the models. Consequently, the selection of the optimal kinetic descriptor was based on the physical consistency between the model-predicted equilibrium capacity (q_{cal}) and the experimental value (q_{exp}) and validated by the lowest AIC and BIC values to minimize information loss.

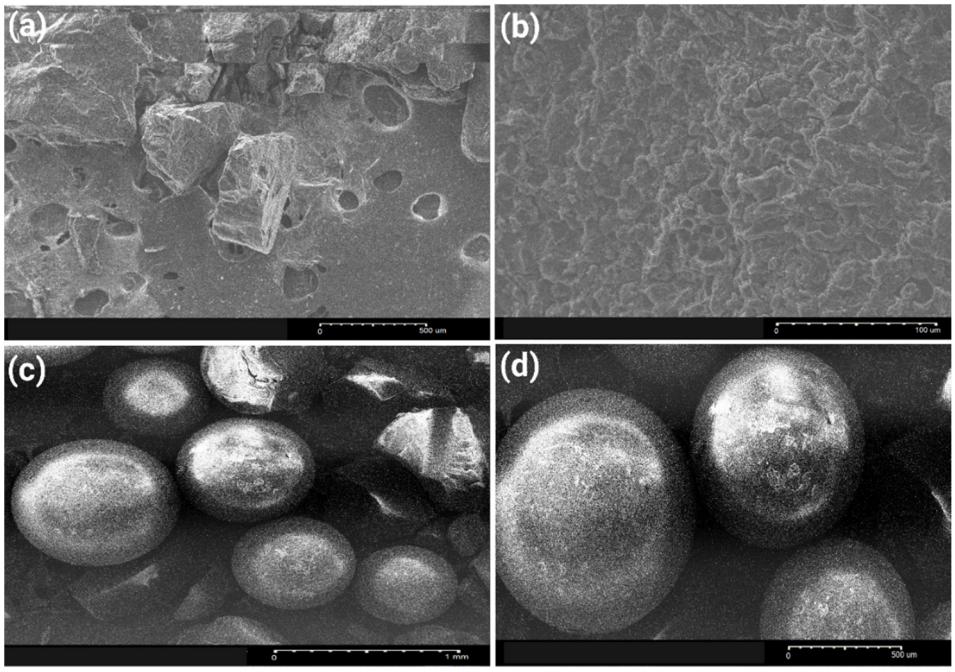

Figure 3. SEM images of (**a**) AC before adsorption, (**b**) AC after adsorption, (**c**) XAD-4 resin before adsorption, and (**d**) XAD-4 resin after adsorption of TPhC from OMWW.

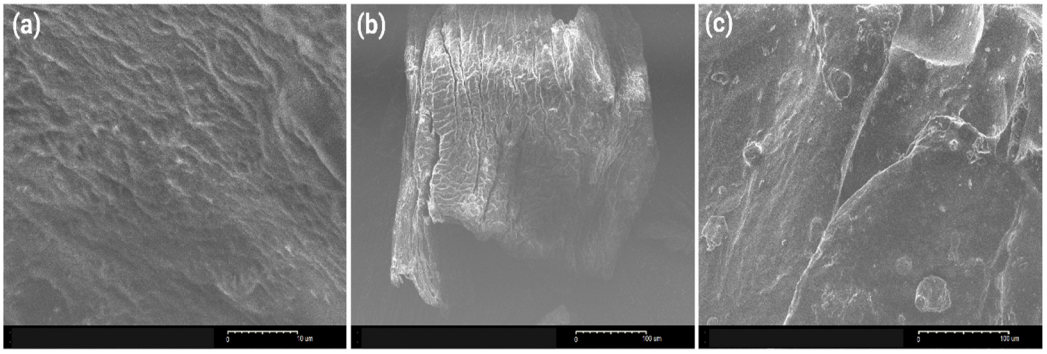

Figure 4. SEM images of (**a**) raw shrimp waste, (**b**) CH-B before, and (**c**) CH-B after adsorption of TPhC from OMWW.

Table 4. Parameters of the kinetic models for the adsorption of TPCs on AC, XAD-4 resin, and CH-B. Values are reported as parameter ± standard error (SE) of the non-linear regression.

Model	Parameters	AC	XAD-4 Resin	CH-B
PFO (Equation (1))	q_1 (mg/g)	84.1 ± 0.8	90.5 ± 3.1	210 ± 6
	K_1 ($\times 10^{-2}$) 1/min	17 ± 2	6.9 ± 0.8	4.2 ± 0.4
	R^2	0.98	0.98	0.99
	AIC	29.7	35.9	42.1
	BIC	23.9	30.1	33.9

Table 4. *Cont.*

Model	Parameters	AC	XAD-4 Resin	CH-B
PSO (Equation (2))	q_2 (mg/g)	89.6 ± 0.9	136.1 ± 0.3	258 ± 20
	K_2 ($\times 10^{-4}$) g/(mg.min)	29.7 ± 2.5	7.6 ± 2.3	1.6 ± 0.5
	R^2	0.99	0.96	0.97
	AIC	16.1	39.2	48.6
	BIC	10.3	24.4	40.4
Elovich (Equation (3))	a (g/mg)	656 ± 592	1615.9 ± 7.6	1514.9 ± 5.9
	b (mg/(g min)	0.10 ± 0.01	0.04 ± 0.01	0.01
	R^2	0.98	0.94	0.95
	AIC	31.8	44.6	52.9
	BIC	26.1	38.8	44.8

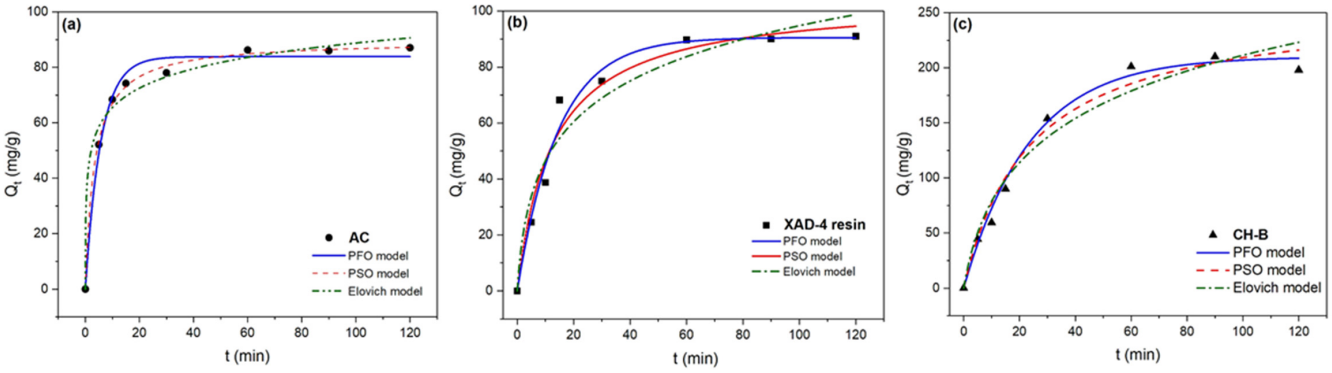

Figure 5. Adsorption Kinetics of TPhC onto (**a**) AC, (**b**) XAD-4 resin, and (**c**) CH-B (pH = 5, T = 25 °C).

For AC, the adsorption equilibrium was reached rapidly, within 45 min, achieving an experimental capacity of 86 mg/g. The kinetic analysis identified the PSO model as the most statistically robust descriptor, exhibiting the lowest AIC (16.5) and BIC (10.3) values compared to the PFO model. Furthermore, the equilibrium capacity predicted by the PSO model (q_2 = 89.6 ± 0.9 mg/g) showed excellent agreement with the experimental data. Moreover, the high pseudo-second-order rate constant (K_2) of (29.7 ± 2.5) × 10^{-4} g/(mg.min) under the PSO model supports the presence of fast external diffusion and high accessibility to microporous structures. This strong PSO fit suggests that the rate-limiting step is governed by surface chemical interactions, likely involving π–π interactions and hydrogen bonding with surface functional groups. These results are consistent with the previous findings of Solomakou and Goula [41], who reported a multilayer and energetically heterogeneous adsorption behavior on activated carbon materials.

In the case of XAD-4 resin, a distinct divergence was observed between the models. While the PSO model provided a mathematically acceptable fit (R^2 = 0.96), it overestimated the equilibrium capacity (q_2 = 136.1 mg/g) that significantly exceeded the experimental value (90.2 mg/g). In contrast, the PFO model demonstrated superior physical consistency, yielding a predicted capacity (q_1 = 90.5 mg/g) nearly identical to the experimental observation. This physical validity is corroborated by the statistical metrics, where the PFO model achieved a lower AIC (35.9) than the PSO model (39.2), along with a moderate rate constant (K1 = (6.9 ± 0.8) × 10^{-2} min^{-1}). This kinetic behavior reflects diffusion-limited physisorption, where the rigid polymeric network of XAD-4 restricts intraparticle diffusion. Given the non-polar, microporous architecture of XAD-4, adherence to PFO kinetics aligns with a physical adsorption mechanism governed fundamentally by intraparticle diffusion. These findings are consistent with Barkakati et al. [42], who similarly reported that adsorption onto XAD-type resins is primarily governed by diffusion-controlled physiosorption due to

the microporous structure of the polymeric matrix. According to Juang and Yeh [43], the ratio of adsorbent pore diameter to adsorbate molecular size determines the predominant adsorption domain, supporting this diffusion-controlled mechanism.

For CH-B, adsorption equilibrium was attained after about 60 min, with an experimental capacity of 205.1 mg/g. The PFO model demonstrated superior performance for this system. It provided a precise prediction of the equilibrium uptake (q_1 = 210 ± 6 mg/g), whereas the PSO model overestimated the capacity (q_2 = 258 ± 20 mg/g). Statistical validation confirmed this superiority, with the PFO model presenting the lowest AIC (42.1) and BIC (33.9) values, indicating minimal information loss relative to the PSO model (AIC = 48.6). This suggests that TPhC uptake by CH-B is likely controlled by the high availability of active sites or external mass transfer limitations, rather than a singular second-order surface reaction. Although Al-Qodah et al. [44] highlighted that biosorption systems involving functionalized biopolymers, such as chitosan derivatives, typically conform to PSO kinetics, Simonin et al. [45] demonstrated that PFO kinetics frequently provide a superior fit for adsorption datasets when rigorous non-linear regression is applied, challenging the widespread dominance of the PSO model. Consequently, the adherence to the PFO model suggests that the adsorption process is driven initially by rapid physical binding and surface-controlled kinetics before chemisorption dominates at later stages.

The Elovich model was also evaluated to examine potential chemisorption kinetics on heterogeneous surfaces. However, it yielded significantly lower correlation coefficients ($R^2 \leq 0.95$) and higher AIC values specifically for XAD-4 and CH-B. This poor fit further confirms that the adsorption mechanism for these two materials is not governed by the specific chemisorption steps described by the Elovich equation, but rather by physical diffusion processes best captured by the PFO model.

In conclusion, integrating the AIC and BIC criteria with physical validation (q_{cal} vs. q_{exp}) enabled a robust differentiation of kinetic mechanisms. The PFO model was selected for XAD-4 and CH-B due to its superior predictive accuracy and consistency with physical diffusion processes. Conversely, the PSO model was confirmed for AC, reflecting its chemisorption-dominated nature.

3.4. Batch Adsorption Isotherms

The equilibrium adsorption data for TPhC were analyzed using the Langmuir, Freundlich, and Temkin isotherm models to characterize the sorption behavior of XAD-4 resin, AC, and CH-B. As illustrated in Figure 6, each of the three adsorbents exhibited distinct adsorption profiles, reflecting differences in surface properties, binding affinities, and interaction mechanisms. The model parameters and statistical error functions, specifically the coefficient of determination (R^2), Akaike Information Criterion (AIC), and Bayesian Information Criterion (BIC), are summarized in Table 5. The analysis of the error functions revealed that relying solely on R^2 is insufficient for robust model discrimination, particularly for AC and CH-B, where correlation coefficients exceeded 0.98 for multiple models. Consequently, model selection was guided by the minimization of AIC and BIC values to identify the model that best describes the data with minimal information loss.

The adsorption on AC presented a case of model equifinality, where the Langmuir, Freundlich, and Temkin models all yielded identical correlation coefficients (R^2 = 0.99), preventing their discrimination. Although relying on a small dataset leading to a risk of over-interpretation, the Akaike Information Criterion suggests a statistical advantage for the Temkin model (lowest AIC of −1.02). This is, however, in agreement with an adsorption process occurring on an energetically heterogeneous surface, a behavior typical of microporous activated carbon with diverse surface functional groups [46]. These findings are consistent with those of Solomakou et al. [47], who reported heterogeneous and multilayer

adsorption on activated carbon. Furthermore, Allahkarami et al. [48] linked this behavior to the high surface functionalization of activated carbons, where diverse active sites create a non-uniform distribution of adsorption energies.

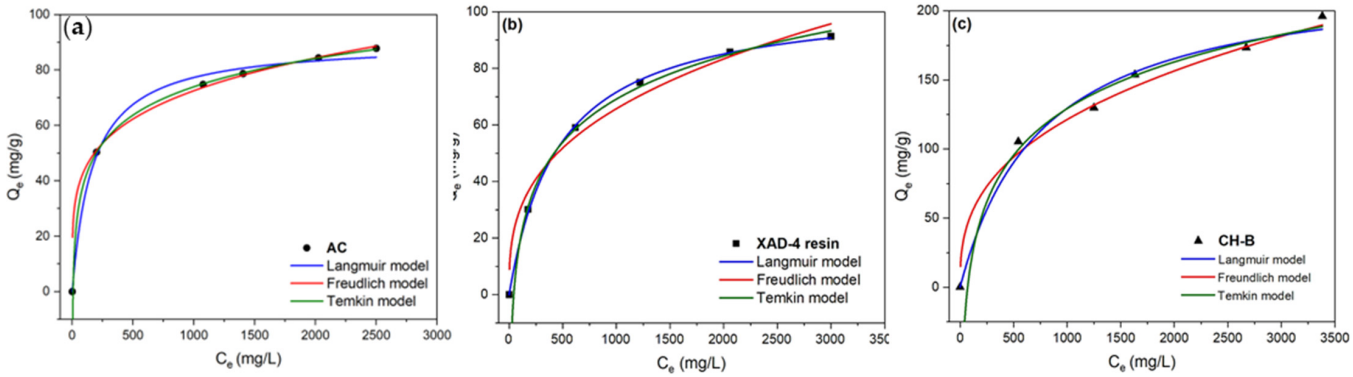

Figure 6. Adsorption isotherms of TPhC onto (**a**) AC, (**b**) XAD-4 resin, and (**c**) CH-B (pH = 5, T = 25 °C).

Table 5. Parameters of the isotherm model for the adsorption of TPhC on AC, XAD-4 resin, and CH-B. Values are reported as parameter ± standard error (SE) of the non-linear regression.

Model	Parameters	AC	XAD-4 Resin	CH-B
Langmuir (Equation (5))	q_m (mg/g)	90.2 ± 2.1	104.8 ± 1.4	229.2 ± 17.3
	K_L ($\times 10^{-3}$) (L/mg)	6.01 ± 0.8	2.11 ± 0.09	1.01 ± 0.32
	R_L	0.01	0.21	0.17
	R^2	0.99	0.99	0.98
	AIC	27.3	14.9	42.6
	BIC	14.6	2.3	30.02
Freundlich (Equation (7))	K_F (mg/g)(L/mg)$^{1/n}$	16.05 ± 1.32	2.36 ± 1.04	11.4 ± 2.6
	1/n	0.22 ± 0.01	0.52 ± 0.08	0.35 ± 0.03
	R^2	0.99	0.96	0.98
	AIC	27.03	44.5	44.9
	BIC	1.8	19.3	19.7
Temkin (Equation (8))	q_T (mg/g)	14.7 ± 0.1	39.3 ± 2.3	48.6 ± 5.04
	K_T ($\times 10^{-2}$) (L/g)	15 ± 0.6	1.0 ± 0.09	1.4 ± 0.5
	R^2	0.99	0.99	0.99
	AIC	−1.02	19.3	39.2
	BIC	−13.6	6.7	26.6

For XAD-4 resin, the experimental data were best fitted by the Langmuir model (R^2 = 0.99), which exhibited the lowest AIC (14.9) and BIC (2.3) values compared to the Temkin (AIC = 19.3) and Freudlich (AIC = 44.5) models. The robustness of the Langmuir equation fits confirms that TPhC adsorption onto XAD-4 resin is governed by a monolayer coverage on a structurally homogeneous surface with energetically equivalent binding sites. This aligns with the resin's non-functionalized, hydrophobic polystyrene–divinylbenzene matrix, where uptake is driven by non-specific hydrophobic interactions rather than heterogeneous chemical binding. The maximum monolayer adsorption capacity (q_m) was determined to be 104.8 ± 1.4 mg/g, with a separation factor (R_L) of 0.21, confirming the favorable nature of the adsorption process. The adsorption behavior observed in this study is in strong agreement with the established literature regarding Amberlite XAD-4. Ku and Lee [7] reported a correlation coefficient (R^2) of 0.98 for the Langmuir isotherm, compared to 0.95 for the Freundlich model, reinforcing the validity of the monolayer coverage theory for this adsorbent-adsorbate system.

Among the tested materials, CH-B demonstrated the highest adsorption potential. Statistical analysis favored the Temkin model, which yielded the lowest AIC (39.2) and BIC (26.7) values compared to the Langmuir and Freundlich models. The adherence to the Temkin equation implies that the surface of the biosorbent is energetically heterogeneous, characterized by a non-uniform distribution of binding energies. This strong interaction is corroborated by a high equilibrium binding energy parameter (q_T = 48.6 mg/g), reflecting the significant affinity of phenolic compounds for the functional groups on the biosorbent surface. This aligns with the work of El-Shafey et al. [49], who similarly attributed the complex adsorption behavior of phenol on chitosan/MCM-48 nanocomposites to the heterogeneous surface structure resulting from material modification. Additionally, Liu et al. [11] noted that the presence of multiple functional groups (amine and hydroxyl) on chitosan surfaces inherently leads to energetic heterogeneity during adsorption of phenolic compounds.

Table 6 presents the performance of phenolic compound adsorption from OMWW on chitosan biosorbent (CH-B) and recent chitosan-based adsorbents published in the literature. Direct quantitative comparison is challenging, as the present study is the only one among those listed to report a full isotherm analysis and a determined maximum adsorption capacity (q_m = 229 mg/g). However, valuable context can be drawn from specific benchmarks. For instance, insect-based chitosan [17] exhibited a higher capacity (416 mg/g), although it was achieved under conditions of lower adsorbent dosage and lower initial concentration of phenolic compounds. Two other studies compared modified chitosan [18] or chitosan composite [19] with unmodified chitosan; in both cases the modification led to increased adsorption capacity. The modified lobster-based chitosan [18] showed a capacity of the order of magnitude of the present unmodified shrimp-based chitosan. It is interesting to note the high capacity of both unmodified shrimp and insect-based chitosans, confirming the interest of their use in treating wastewaters such as OMWW.

Table 6. Phenolic compound (PC) adsorption performance of various chitosan-based adsorbents and composites reported in the recent literature. Adsorption capacity in the conditions of the test (Q_{exp}) and maximum adsorption capacity from isotherms (Q_{max}).

Adsorbent	Precursor/ Modification	Capacity		Initial Conc. of TPhC (C_0, mg/L)	Dosage (g/L)	Reference
		Q_{exp} (mg/g)	Q_{max} (mg/g)			
Chitosan Biosorbent (CH-B)	Shrimp Shells (Unmodified)	196	229	3765	2	This Study
Unmodified Insect Chitosan (*H. illucens*)	*Hermetia illucens* Waste	416		269	0.5	Elouali et al. [17]
Chitosan	Lobster wastes (Unmodified, CS)	83		8210	30	Belhadj et al. [18]
	chitosan–epichlorohydrin bead (CS-ECH)	232.6				
Chitosan Nanocomposite	Commercial Unmodified Chitosan	15		228	10	Shmeis et al. [19]
	Nanocomposite (CKI-CP)	19.8			2	

In summary, the combined statistical and mechanistic evaluation supports distinct adsorption behaviors: energetically heterogeneous for AC and CH-B versus homogeneous for XAD-4. Crucially, CH-B was identified as the most efficient material, exhibiting the

highest adsorption capacity for phenolic compounds and significantly outperforming both commercial adsorbents.

3.5. Adsorption Performance, Process Modeling, and Optimization by Response Surface Methodology

3.5.1. Model Adequacy Checking and Statistical Analysis

In the study, the adsorption yield of TPhC using AC, XAD-4 resin, and CH-B adsorbents was evaluated through RSM based on the Box–Behnken design (BBD), considering temperature, pH, and adsorbent dosage as key operational parameters. The analysis of variance (ANOVA) was applied to validate the regression models and assess the influence of each factor, with the main results summarized in Table 7. Adequate precision (A.P) compares the predicted signal to the experimental noise, coefficient of variation (C.V) indicates the model's reproducibility, and desirability is a multi-response optimization index ranging from 0 to 1. Detailed ANOVA outputs, including F-values and *p*-values for all terms, are reported in Supplementary Table S3. All three regression models were statistically significant ($p < 0.05$), with F-values exceeding 4.9 and adequate precision values (AP > 4), confirming an acceptable signal-to-noise adequacy of the design. Coefficients of determination ($R^2 > 0.90$) further supported model reliability, although the coefficients of variation (CV) highlighted variability in robustness among the adsorbents [50].

Table 7. Analysis of variance of optimization models when polyphenol adsorption yield is maximized using AC, XAD-4 resin, and CH-B adsorbents.

Adsorbent	Reduced Equation	R^2	A.P	S.D	C.V
AC	$Y1 = 58.92 - 1.61A - 11.54B + 16.27C + 4.39AB - 0.58AC + 0.88BC - 0.14A^2 + 8.35B2 + 1.33C^2 + 10.66A^2B$	0.96	9.15	4.94	7.87
XAD-4 resin	$Y2 = 85.15 + 3.17A + 53.47B + 0.91C - 1.44AB - 0.02AC - 0.02BC + 0.028A^2 - 4.88B2 - 0.0006C^2 + 0.14AB^2$	0.94	9.39	3.63	5.68
CH-B	$Y3 = 63.38 + 2.20A + 0.4812B - 2.67C + 2.97AB + 0.77AC + 5.59BC - 20.01A^2 + 7.08B^2 - 0.46C^2 + 3.35A^2B - 1.48A^2C$	0.99	37.77	1.25	2.22

The fitted regression model for AC was statistically significant (F = 8.85, $p = 0.0250$), with a non-significant lack of fit ($p = 0.8554$), indicating acceptable model adequacy. The most influential factor was adsorbent dosage (F = 61.77, $p = 0.0014$), while pH and temperature were not statistically significant within the tested range. Model evaluation metrics confirmed a good fit with $R^2 = 0.96$, A.P. = 9.15, S.D. = 4.94, and CV = 7.87%, suggesting acceptable precision and moderate variability.

The XAD-4 resin model presented a more complex behavior, incorporating both linear and interaction effects. strong reliability ($R^2 = 0.94$) with acceptable reproducibility (CV = 5.68%). The regression equation was significant (F = 6.11, $p = 0.0480$), and the lack of fit was not significant ($p = 0.6782$). Key influencing factors included pH (F = 12.40, $p = 0.0244$) and adsorbent dosage (F = 11.64, $p = 0.0270$), while interaction terms AB (F = 9.60, $p = 0.0363$) and AC (F = 31.10, $p = 0.0051$) also played a significant role. The complexity of the adsorption mechanism was further evidenced by the significance of the quadratic coefficient B2 (F = 16.10, $p = 0.016$) and the reduced cubic interaction term AB^2 (F = 12.53, $p = 0.024$). The statistical significance of this asymmetric term validates the non-linearity described by the reduced cubic model (Equation (9)) and indicates that the effect of temperature (B) is strictly dependent on the pH level (A). The statistical adequacy was supported by $R^2 = 0.94$, A.P. = 9.39, S.D. = 3.63, and CV = 5.68%, confirming a reliable and reproducible model.

The model developed for CH-B demonstrated the highest statistical robustness and complexity among all the adsorbents. The regression was highly significant (F = 119.11, p = 0.0011), and the lack of fit was not statistically significant (p = 0.0908). Significant contributions came from temperature (F = 24.79, p = 0.0156), interaction terms AB (F = 22.60, p = 0.0177) and BC (F = 80.21, p = 0.0029), and especially quadratic terms such as A^2 (F = 948.51, $p < 0.0001$) and B^2 (F = 118.77, p = 0.0017).

Regarding the CH-B adsorbent, the stepwise regression analysis revealed significant higher-order interactions, specifically the cubic term AB^2 (F = 14.43, p = 0.032). Retaining this term in the modified polynomial was critical for enhancing the model's predictive accuracy. The model's statistical descriptors were excellent, with R^2 = 0.99, A.P. = 37.77, S.D. = 1.25, and CV = 2.22%, confirming its high accuracy, low variability, and outstanding predictive ability.

3.5.2. Analysis of Process Interactions and Optimization of Operating Conditions

The three-dimensional response surface plots derived from the Box–Behnken design are illustrated in Figure 7. These plots showcase the interactive effects of temperature, pH, and adsorbent dosage on the adsorption yield of TPhC onto XAD-4 resin, AC, and CH-B, respectively. Table 8 summarizes the optimal operating conditions determined via the desirability function for each adsorbent. The surface plots reveal distinctive response topographies for each adsorbent, reflecting differences in their physicochemical characteristics and underlying adsorption mechanisms.

Table 8. Optimal experimental conditions obtained by the desirability function for maximizing TPhC adsorption yield.

Adsorbent	Temperature (°C)	pH	Dosage (g/L)	TPhC Yield (%)	Desirability
AC	49	7	100	80	1
XAD-4 resin	25	4.93	100	79	0.98
CH-B	39	2	2	78	0.96

For AC, the response surfaces exhibited predominantly linear profiles, with adsorption yields increasing steadily with dosage. In contrast, the surfaces remained relatively flat with respect to pH and temperature, indicating limited sensitivity to these parameters within the tested range. Numerical optimization yielded a maximum desirability score of 1.0. The optimal conditions were identified as 49 °C, pH 7, and a dosage of 100 g/L, resulting in a maximum TPhC adsorption yield of 80%.

These findings confirm that AC primarily operates through non-specific, physical adsorption mechanisms, driven by its high surface area and porous structure rather than specific chemical interactions. Such behavior aligns with previous studies that emphasize the non-specific yet reliable adsorption behavior of activated carbon. Mojoudi et al. [8] observed similar results, indicating that adsorption capacity increases linearly with the availability of surface area. Similarly, Nguyen et al. [51] highlighted that AC shows effectiveness across a broad pH range; however, it lacks selectivity, resulting in the adsorption of both target pollutants and biodegradable co-substrates. This behavior underscores the physical nature of adsorption onto AC, which is primarily influenced by its specific surface area and porous structure, rather than by particular chemical affinities or environmental factors.

In the case of XAD-4 resin, the response surface plots reveal significant curvature, particularly in the interaction between pH and adsorbent dosage. This suggests that the adsorption efficiency is not only dependent on individual factors but is also significantly influenced by their synergistic effects. The most prominent effect is observed in the pH–dosage surface, where higher adsorption yields are attained at low pH and high adsorbent

dosage (up to 100 g/L), reflecting strong acid-dependent adsorption behavior. The optimal conditions determined by the desirability function were 25 °C, pH 4.93, and 100 g/L dosage, achieving a predicted TPhC yield of 78.81% and a desirability of 0.98. This is supported by the findings of Petrotos et al. [37] and Ku and Lee [52], who demonstrated that XAD-4 resin exhibits increased affinity for polyphenols under acidic conditions. This behavior is attributed to the state of the phenolic hydroxyl groups at low pH. By maintaining these groups in their protonated (neutral) form, the solubility of the phenolic compounds is reduced, thereby promoting hydrophobic interactions with the non-polar polystyrene–divinylbenzene matrix of the resin. Furthermore, the positive effect of dosage confirms that increasing the mass of resin provides a greater number of active sites, effectively overcoming saturation limitations.

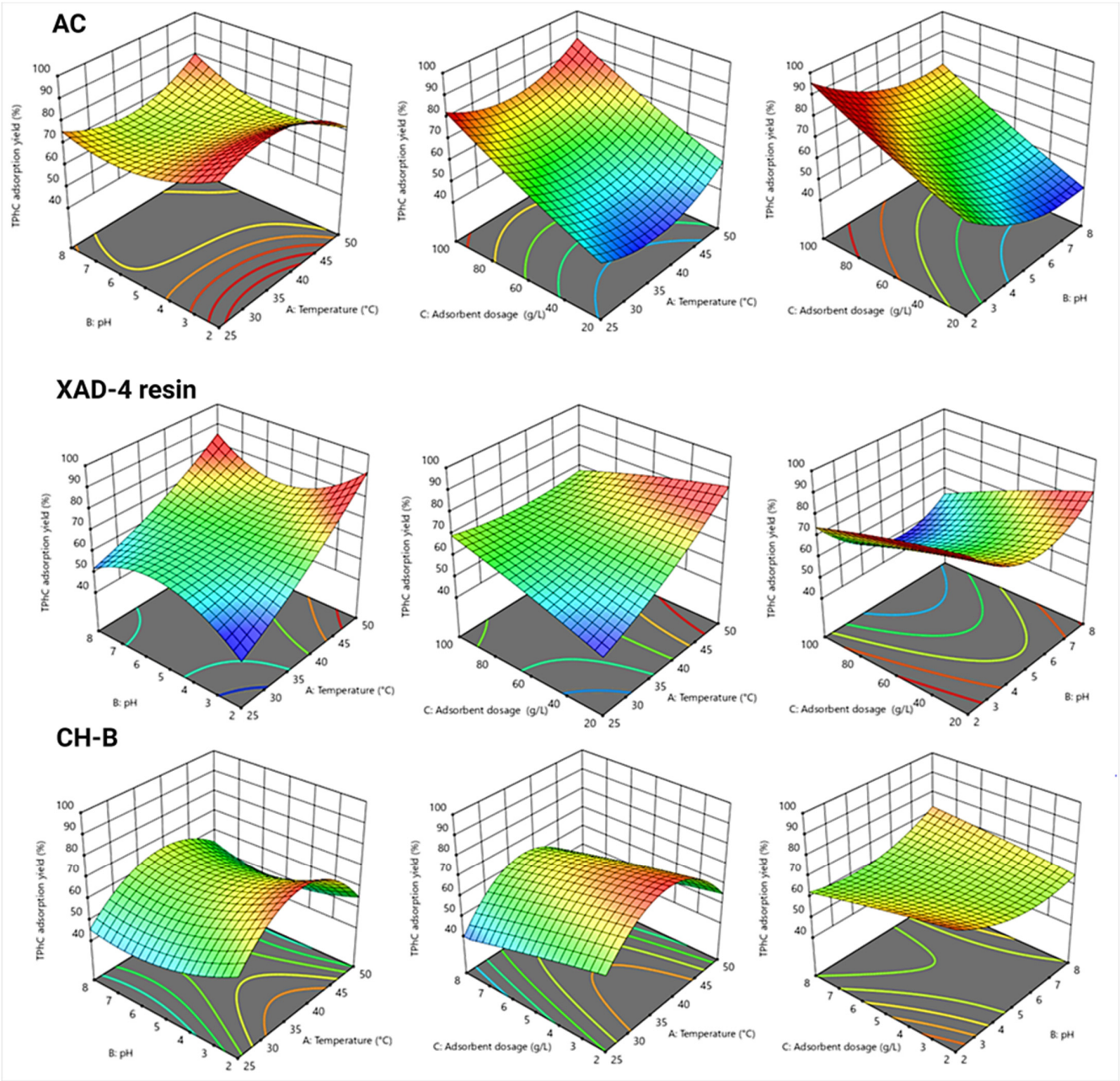

Figure 7. Response surface 3D plots of TPhC adsorption yield (%) into AC, XAD-4 resin, and CH-B.

The response surface plots for CH-B demonstrate pronounced non-linearities, indicating strong interactions between operational parameters. In particular, the temperature–pH

and temperature–dosage plots reveal significant curvature. The effects of temperature and pH were particularly pronounced. In particular, the high impact of pH with high adsorption yields at acidic pH aligns with previous studies [26,52], which demonstrated that chitosan-based adsorbents exhibit strong binding capacity under acidic conditions due to the protonation of amine groups. The process optimization revealed that a relatively low dosage of 2 g/L was sufficient to achieve a maximum adsorption yield of 78% low pH of 2 and moderate temperatures of 39 °C (desirability = 0.96). This result was unexpected, as conventional adsorption theory suggests that increasing adsorbent dosage typically enhances removal efficiency due to the increased availability of active sites.

However, in the studied experimental domain, the RSM statistical analysis indicated that the main effect of the adsorbent dosage factor was non-significant on the TPhC removal yield, as confirmed by the relatively flat shape of the response surface curves along the dosage axis. A plausible explanation for this phenomenon may be the agregation of particules at high dosage, which was previ-ously described in the literature as the 'solid concentration effect' [53,54]. At high solid loads, particle overcrowding can lead to the formation of clusters. This would reduce the total surface area available for mass transfer and make the active sites located deep inside these aggregates inaccessible to the adsorbate molecules. However, as morphological analysis of aggregates was not carried out in this study, this explanation remains a strong hypothesis and should be confirmed withby further researchexperimental evidence.

4. Conclusions

This study identifies the chitosan biosorbent (CH-B) as an efficient and sustainable alternative to commercial activated carbon and synthetic resins for the recovery of TPhC from OMWW. Mechanistic analysis reveals that the enhanced performance of CH-B is driven by adsorption on an energetically heterogeneous surface, facilitated by the abundant -NH2 and -OH functional groups. The conformity of CH-B adequacy to the PFO model suggests a process governed by diffusion limitations or active site availability ra-ther than simple surface reaction steps. While commercial adsorbents demonstrated effective uptake governed by chemisorption (AC) and hydrophobic retention (XAD-4), the thermodynamic and kinetic properties of bio-based CH-B highlight its superior potential. Consequently, the deployment of CH-B offers a dual advantage: valorizing a biopolymer waste stream while efficiently detoxifying complex industrial effluents. Future research should focus on the regeneration capacity and long-term stability of CH-B, alongside an assessment of the economic feasibility for its industrial-scale implementation. While these results confirm the robustness of CH-B in a real matrixHowever, the unexpected high re-moval efficiencies at low CH-B dosages with the hypothetic explanation of particle aggre-gation at high dosages needs further investigation. Future studies should focus on hydro-dynamic particle size analysis and microscopic observations to experimentally confirm the physical mechanisms limiting adsorption efficiency at high solid concentrations. Ad-ditionally, further experimental studies are required to quantify the specific interference and competition of sugars and lipids in this multicomponent system. Finally, assessing the regeneration capacity, long-term stability, and economic feasibility of CH-B will be crucial for its deployment in real-world wastewater treatment scenarios.

Supplementary Materials: The following supporting information can be downloaded at https://www.mdpi.com/article/10.3390/app16031231/s1. Table S1: Experimental and predicted TPhC adsorption yields (%) for XAD-4 resin and activated carbon; Table S2: Experimental and predicted TPhC adsorption yields (%) for CH-B; Table S3: Statistical parameters of the fitted RSM models for TPhC adsorption yield by AC, XAD-4 resin, and CH-B.

Author Contributions: Conceptualization. C.H., M.N. and H.C.; methodology. C.H., M.N. and H.C.; software. C.H.; validation. C.H., M.N., A.B., J.H. and H.C.; formal analysis. C.H., H.C., J.H., S.T. and H.C.; investigation. C.H., A.E., S.T. and M.N.; resources. M.N., A.B. and H.C.; data curation. C.H., A.B., J.H. and H.C.; writing—original draft preparation. C.H.; writing—review and editing. C.H., M.N., A.B., J.H., R.E. and H.C.; visualization. C.H., S.T. and A.E.; supervision. H.C., A.B., J.H. and M.N.; project administration. H.C., M.N. and J.H.; funding acquisition. J.H. and M.N. All authors have read and agreed to the published version of the manuscript.

Funding: This research was supported by the Franco-Moroccan bilateral program PHC TOUBKAL 2023 (Grant No. 12345AB).

Institutional Review Board Statement: Not applicable.

Informed Consent Statement: Not applicable.

Data Availability Statement: The original contributions presented in this study are included in the article and Supplementary Material. Further inquiries can be directed to the corresponding authors.

Acknowledgments: The authors acknowledge support from the Centre National pour la Recherche Scientifique et Technique (CNRST) through the "PhD-Associate Scholarship—PASS" program initiated in 2024. Experimental work was carried out at the Laboratory of Bioresources, Biotechnology, Ethnopharmacology, and Health, University Mohammed First, Oujda, Morocco. During the preparation of this work, the author(s) used Gemini in order to improve the readability and language quality of the manuscript. After using this tool/service, the author(s) reviewed and edited the content as needed and take(s) full responsibility for the content of the publication.

Conflicts of Interest: The authors declare that they have no conflicts of interest.

References

1. International Olive Council (IOC). World Olive Oil Figures—2023/24 Season. 2024. Available online: https://www.internationaloliveoil.org/what-we-do/economic-affairs-promotion-unit/#figures (accessed on 10 October 2024).
2. Vaz, T.; Quina, M.M.J.; Martins, R.C.; Gomes, J. Olive Mill Wastewater Treatment Strategies to Obtain Quality Water for Irrigation: A Review. *Sci. Total Environ.* **2024**, *931*, 172676. [CrossRef]
3. Dermeche, S.; Nadour, M.; Larroche, C.; Moulti-Mati, F.; Michaud, P. Olive Mill Wastes: Biochemical Characterizations and Valorization Strategies. *Process Biochem.* **2013**, *48*, 1532–1552. [CrossRef]
4. Dich, A.; Abdelmoumene, W.; Belyagoubi, L.; Assadpour, E.; Belyagoubi Benhammou, N.; Zhang, F.; Jafari, S.M. *Olive Oil Wastewater: A Comprehensive Review on Examination of Toxicity, Valorization Strategies, Composition, and Modern Management Approaches*; Springer: Berlin/Heidelberg, Germany, 2025; ISBN 1135602536127.
5. Lin, S.H.; Juang, R.S. Adsorption of Phenol and Its Derivatives from Water Using Synthetic Resins and Low-Cost Natural Adsorbents: A Review. *J. Environ. Manag.* **2009**, *90*, 1336–1349. [CrossRef]
6. Girometti, E.; Frascari, D.; Pinelli, D.; Di Federico, V.; Libero, G.; Ciriello, V. Polyphenol Adsorption and Recovery from Olive Mill Wastewater: A Model Reduction-Based Optimization and Economic Assessment. *J. Environ. Chem. Eng.* **2025**, *13*, 116370. [CrossRef]
7. Ku, Y.; Lee, K.C. Removal of Phenols from Aqueous Solution by XAD-4 Resin. *J. Hazard. Mater.* **2000**, *80*, 59–68. [CrossRef] [PubMed]
8. Mojoudi, N.; Mirghaffari, N.; Soleimani, M.; Shariatmadari, H.; Belver, C.; Bedia, J. Phenol Adsorption on High Microporous Activated Carbons Prepared from Oily Sludge: Equilibrium, Kinetic and Thermodynamic Studies. *Sci. Rep.* **2019**, *9*, 19352. [CrossRef] [PubMed]
9. Cui, C.; Li, D.; Wang, L.j. Functionalized Nanocomposite Biopolymer-Based Environmental-Friendly Adsorbents: Design, Adsorption Mechanism, Regeneration, and Degradation. *Sep. Purif. Technol.* **2025**, *363*, 132034. [CrossRef]
10. Salehi, E.; Daraei, P.; Arabi Shamsabadi, A. A Review on Chitosan-Based Adsorptive Membranes. *Carbohydr. Polym.* **2016**, *152*, 419–432. [CrossRef]
11. Liu, C.; Crini, G.; Lichtfouse, E.; Wilson, L.D.; Picos-Corrales, L.A.; Balasubramanian, P.; Li, F. Chitosan-Based Materials for Emerging Contaminants Removal: Bibliometric Analysis, Research Progress, and Directions. *J. Water Process Eng.* **2025**, *71*, 107327. [CrossRef]
12. Vinayagam, V.; Murugan, S.; Kumaresan, R.; Narayanan, M.; Sillanpää, M.; Viet N Vo, D.; Kushwaha, O.S.; Jenis, P.; Potdar, P.; Gadiya, S. Sustainable Adsorbents for the Removal of Pharmaceuticals from Wastewater: A Review. *Chemosphere* **2022**, *300*, 134597. [CrossRef]

13. Akhtar, J.; Amin, N.A.S.; Shahzad, K. A Review on Removal of Pharmaceuticals from Water by Adsorption. *Desalin. Water Treat.* **2016**, *57*, 12842–12860. [CrossRef]
14. Cruz-Reina, L.J.; Rodríguez-Cortina, J.; Vaillant, F.; Herrera-Orozco, I.; Carazzone, C.; Sierra, R. Extraction of Fermentable Sugars and Phenolic Compounds from Colombian Cashew (*Anacardium occidentale*) Nut Shells Using Subcritical Water Technology: Response Surface Methodology and Chemical Profiling. *Chem. Eng. J. Adv.* **2024**, *20*, 100661. [CrossRef]
15. Fseha, Y.H.; Shaheen, J.; Sizirici, B. Phenol Contaminated Municipal Wastewater Treatment Using Date Palm Frond Biochar: Optimization Using Response Surface Methodology. *Emerg. Contam.* **2023**, *9*, 100202. [CrossRef]
16. Elayadi, F.; Boumya, W.; Achak, M.; Chhiti, Y.; Alaoui, F.E.M.; Barka, N.; Adlouni, C.E. Experimental and Modeling Studies of the Removal of Phenolic Compounds from Olive Mill Wastewater by Adsorption on Sugarcane Bagasse. *Environ. Challenges* **2021**, *4*, 100184. [CrossRef]
17. Elouali, S.; Ait Hamdan, Y.; Benali, S.; Lhomme, P.; Gosselin, M.; Raquez, J.M.; Rhazi, M. Extraction of Chitin and Chitosan from *Hermetia illucens* Breeding Waste: A Greener Approach for Industrial Application. *Int. J. Biol. Macromol.* **2025**, *285*, 138302. [CrossRef] [PubMed]
18. Belhadj, R.; Labidi, A.; Salaberria, A.M.; Labidi, J. Comparative Adsorption of Anionic Dye Congo Red and Purification of Olive Mill Wastewater by Chitin and Their Derivatives. *Desalin. Water Treat.* **2021**, *220*, 392–408. [CrossRef]
19. Shmeis, R.M.A.; Tarawneh, I.N.; Issa, A.T. Removal of Phenolic Compounds from Olive Mill Wastewater Using Chitosan/Kaolinite/Iron Oxide Nanocomposites. *Water Sci. Technol.* **2025**, *92*, 1360–1378. [CrossRef]
20. Dahmane, E.M.; Taourirte, M.; Eladlani, N.; Rhazi, M. Extraction and Characterization of Chitin and Chitosan from Parapenaeus Longirostris from Moroccan Local Sources. *Int. J. Polym. Anal. Charact.* **2014**, *19*, 342–351. [CrossRef]
21. Elalami, D.; Carrère, H.; Abdelouahdi, K.; Oukarroum, A.; Dhiba, D.; Arji, M.; Barakat, A. Combination of Dry Milling and Separation Processes with Anaerobic Digestion of Olive Mill Solid Waste: Methane Production and Energy Efficiency. *Molecules* **2018**, *23*, 3295. [CrossRef]
22. Turkmen, N.; Sari, F.; Velioglu, Y.S. Effects of Extraction Solvents on Concentration and Antioxidant Activity of Black and Black Mate Tea Polyphenols Determined by Ferrous Tartrate and Folin-Ciocalteu Methods. *Food Chem.* **2006**, *99*, 835–841. [CrossRef]
23. Azizian, S. Kinetic Models of Sorption: A Theoretical Analysis. *J. Colloid Interface Sci.* **2004**, *276*, 47–52. [CrossRef]
24. Ho, Y.S. Review of Second-Order Models for Adsorption Systems. *J. Hazard. Mater.* **2006**, *136*, 681–689. [CrossRef] [PubMed]
25. Wu, F.C.; Tseng, R.L.; Juang, R.S. Characteristics of Elovich Equation Used for the Analysis of Adsorption Kinetics in Dye-Chitosan Systems. *Chem. Eng. J.* **2009**, *150*, 366–373. [CrossRef]
26. Kumar, N.S.; Subbaiah, M.V.; Reddy, A.S.; Krishnaiah, A. Biosorption of Phenolic Compounds from Aqueous Solutions onto Chitosan-Abrus Precatorius Blended Beads. *J. Chem. Technol. Biotechnol.* **2009**, *84*, 972–981. [CrossRef]
27. Foo, K.Y.; Hameed, B.H. Insights into the Modeling of Adsorption Isotherm Systems. *Chem. Eng. J.* **2010**, *156*, 2–10. [CrossRef]
28. Mudhoo, A. Unveiling New Insights: Revised Temkin Adsorption Isotherm Parameters from Fresh Curve Fits in Adsorption Studies. *Chem. Eng. Sci.* **2025**, *311*, 121585. [CrossRef]
29. Nguyen, H.; You, S.; Hosseini-bandegharaei, A. Mistakes and Inconsistencies Regarding Adsorption of Contaminants from Aqueous Solutions: A Critical Review. *Water Res.* **2017**, *120*, 88–116. [CrossRef]
30. Vareda, J.P. On Validity, Physical Meaning, Mechanism Insights and Regression of Adsorption Kinetic Models. *J. Mol. Liq.* **2023**, *376*, 121416. [CrossRef]
31. Shahkouhmahali, E.; Mohamadzadeh, J. Optimization of Phenolic Compounds Extraction from Olive Mill Wastewater Using Response Surface Methodology. *Water Sci. Technol.* **2023**, *88*, 2400–2408. [CrossRef]
32. Turkyilmaz, H.; Kartal, T.; Yildiz, S.Y. Environmental Health Optimization of Lead Adsorption of Mordenite by Response Surface Methodology: Characterization and Modification. *J. Environ. Health Sci. Eng.* **2014**, *12*, 5. [CrossRef]
33. Víctor-Ortega, M.D.; Ochando-Pulido, J.M.; Airado-Rodríguez, D.; Martínez-Férez, A. Experimental Design for Optimization of Olive Mill Wastewater Final Purification with Dowex Marathon C and Amberlite IRA-67 Ion Exchange Resins. *J. Ind. Eng. Chem.* **2016**, *34*, 224–232. [CrossRef]
34. Fleyfel, L.M.; Leitner, N.K.V.; Deborde, M.; Matta, J.; El Najjar, N.H. Olive Oil Liquid Wastes–Characteristics and Treatments: A Literature Review. *Process Saf. Environ. Prot.* **2022**, *168*, 1031–1048. [CrossRef]
35. Grace Pavithra, K.; Sundar Rajan, P.; Arun, J.; Brindhadevi, K.; Hoang Le, Q.; Pugazhendhi, A. A Review on Recent Advancements in Extraction, Removal and Recovery of Phenols from Phenolic Wastewater: Challenges and Future Outlook. *Environ. Res.* **2023**, *237*, 117005. [CrossRef] [PubMed]
36. Hamadneh, I.; Abu-Zurayk, R.A.; Al-Dujaili, A.H. Removal of Phenolic Compounds from Aqueous Solution Using $MgCl_2$-Impregnated Activated Carbons Derived from Olive Husk: The Effect of Chemical Structures. *Water Sci. Technol.* **2020**, *81*, 2351–2367. [CrossRef] [PubMed]
37. Petrotos, K.B.; Gkoutsidis, P.E.; Kokkora, M.I.; Giankidou, K.G.; Tsagkarelis, A.G. A Study on the Kinetics of Olive Mill Wastewater (OMWW) Polyphenols Adsorption on the Commercial XAD4 Macroporous Resin. *Desalin. Water Treat.* **2013**, *51*, 2021–2029. [CrossRef]

38. Bhatnagar, A.; Sillanpää, M. Applications of Chitin- and Chitosan-Derivatives for the Detoxification of Water and Wastewater—A Short Review. *Adv. Colloid Interface Sci.* **2009**, *152*, 26–38. [CrossRef]
39. Hernández-Barreto, D.F.; Giraldo, L.; Moreno-Piraján, J.C. Dataset on Adsorption of Phenol onto Activated Carbons: Equilibrium, Kinetics and Mechanism of Adsorption. *Data Brief* **2020**, *32*, 106312. [CrossRef]
40. Rinaudo, M. Chitin and Chitosan: Properties and Applications. *Prog. Polym. Sci.* **2006**, *31*, 603–632. [CrossRef]
41. Solomakou, N.; Goula, A.M. Treatment of Olive Mill Wastewater by Adsorption of Phenolic Compounds. *Rev. Environ. Sci. Biotechnol.* **2021**, *20*, 839–863. [CrossRef]
42. Barkakati, P.; Begum, A.; Das, M.L.; Rao, P.G. Adsorptive Separation of Ginsenoside from Aqueous Solution by Polymeric Resins: Equilibrium, Kinetic and Thermodynamic Studies. *Chem. Eng. J.* **2010**, *161*, 34–45. [CrossRef]
43. Juang, R.S.; Yeh, C.L. Adsorptive Recovery and Purification of Prodigiosin from Methanol/Water Solutions of Serratia Marcescens Fermentation Broth. *Biotechnol. Bioprocess Eng.* **2014**, *19*, 159–168. [CrossRef]
44. Al-Qodah, Z.; Al-Zoubi, H.; Hudaib, B.; Omar, W.; Soleimani, M.; Abu-Romman, S.; Frontistis, Z. Sustainable vs. Conventional Approach for Olive Oil Wastewater Management: A Review of the State of the Art. *Water* **2022**, *14*, 1695. [CrossRef]
45. Simonin, J.P. On the Comparison of Pseudo-First Order and Pseudo-Second Order Rate Laws in the Modeling of Adsorption Kinetics. *Chem. Eng. J.* **2016**, *300*, 254–263. [CrossRef]
46. Mishra, L.; Paul, K.K.; Jena, S. Adsorption Isotherm, Kinetics and Optimization Study by Box Behnken Design on Removal of Phenol from Coke Wastewater Using Banana Peel (*Musa* Sp.) Biosorbent. *Theor. Found. Chem. Eng.* **2022**, *56*, 1189–1203. [CrossRef]
47. Solomakou, N.; Tsafrakidou, P.; Goula, A.M. Holistic Exploitation of Spent Coffee Ground: Use as Biosorbent for Olive Mill Wastewaters After Extraction of Its Phenolic Compounds. *Water. Air. Soil Pollut.* **2022**, *233*, 173. [CrossRef]
48. Allahkarami, E.; Dehghan Monfared, A.; Silva, L.F.O.; Dotto, G.L. Lead Ferrite-Activated Carbon Magnetic Composite for Efficient Removal of Phenol from Aqueous Solutions: Synthesis, Characterization, and Adsorption Studies. *Sci. Rep.* **2022**, *12*, 10718. [CrossRef]
49. Fathy, M.; Selim, H.; Shahawy, A.E.L. Chitosan/MCM-48 Nanocomposite as a Potential Adsorbent for Removing Phenol from Aqueous Solution. *RSC Adv.* **2020**, *10*, 23417–23430. [CrossRef]
50. Liu, W.; Yin, P.; Liu, X.; Qu, R. Design of an Effective Bifunctional Catalyst Organotriphosphonic Acid-Functionalized Ferric Alginate (ATMP-FA) and Optimization by Box-Behnken Model for Biodiesel Esterification Synthesis of Oleic Acid over ATMP-FA. *Bioresour. Technol.* **2014**, *173*, 266–271. [CrossRef]
51. Nguyen, V.T.; Nguyen, T.B.; Huang, C.P.; Chen, C.W.; Bui, X.T.; Dong, C. Di Alkaline Modified Biochar Derived from Spent Coffee Ground for Removal of Tetracycline from Aqueous Solutions. *J. Water Process Eng.* **2021**, *40*, 101908. [CrossRef]
52. Li, J.M.; Meng, X.G.; Hu, C.W.; Du, J. Adsorption of Phenol, p-Chlorophenol and p-Nitrophenol onto Functional Chitosan. *Bioresour. Technol.* **2009**, *100*, 1168–1173. [CrossRef]
53. Ghorbani, F.; Younesi, H.; Mahmoud, S.; Akbar, A.; Amini, M.; Daneshi, A. Application of Response Surface Methodology for Optimization of Cadmium Biosorption in an Aqueous Solution by Saccharomyces Cerevisiae. *Chem. Eng. J.* **2008**, *145*, 267–275. [CrossRef]
54. Garg, V.K.; Gupta, R.; Yadav, A.B.; Kumar, R. Dye Removal from Aqueous Solution by Adsorption on Treated Sawdust. *Bioresour. Technol.* **2003**, *89*, 121–124. [CrossRef]